FEATURE ARTICLE

In Situ Infrared Spectroscopy at Single-Crystal Metal Electrodes: An Emerging Link between Electrochemical and Ultrahigh-Vacuum Surface Science

Si-Chung Chang† and Michael J. Weaver*

Department of Chemistry, Purdue University, West Lafayette, Indiana 47907 *(Received: January 14, 1991)*

The utilization of infrared reflection-absorption spectroscopy for the in situ molecular characterization of monocrystalline metal-solution interfaces is outlined in comparison with the behavior of metal surfaces in ultrahigh vacuum (uhv) and illustrated for the adsorption of carbon monoxide on low-index platinum and rhodium surfaces in aqueous media. The effects of altering the electrode potential on the C-O stretching frequencies (ν_{CO}) and terminal/bridging binding-site geometries are discussed in relation to similar spectral changes induced at metal-uhv interfaces by alterations in the local electric field and by the addition of dipolar and ionizable adsorbates. Quantitative links between these electrochemical and uhv-based phenomena are established by utilizing a common surface-potential scale. Interpretation of the various potential-induced spectral shifts is outlined in terms of alterations in the local electrostatic field and in the adsorbate-surface coordinate binding; the need to incorporate the latter phenomenon in order to account for the present experimental results is emphasized. The inherently coupled nature of the solvent dipolar and free charge contributions to the electrochemical surface potential is pointed out. The role of water and hydrogen coadsorption in the electrochemical systems is explored both on the basis of in situ infrared data and from related spectral observations at metal-uhv interfaces. Alterations in CO binding induced by metal coadsorption are briefly noted. The prospects for utilizing infrared spectroscopy to interconnect more generally the structural properties of related metal-solution and metal-uhv interfaces are discussed, along with the value of electrochemical systems for exploring fundamental issues relevant to both types of surfaces.

Introduction

A major ongoing trend in surface electrochemistry is the increasing utilization of spectroscopic and other microscopic techniques for the molecular structural and compositional characterization of metal-solution interfaces. A number of these methods involve emersion of the electrode from the electrolyte and transferral into an ultrahigh-vacuum (uhv) environment.[1] While such "ex situ" approaches allow a wide range of uhv surface characterization techniques to be employed, they can be limited by the changes in surface state that attend electrode transfer. Although more restricted in scope, several "in situ" spectroscopic techniques have been developed in recent years which enable the metal-solution interface to be characterized under electrode potential control, including conditions where electrochemical reactions are proceeding.

Prominent among these methods are Raman[2] and infrared spectroscopies.[3] To date, most electrochemical applications of the former technique have involved conditions where surface-enhanced Raman scattering (SERS) is operative. This offers the unique advantage of the tremendous sensitivity and selectivity of SERS to interfacial versus bulk-phase solution species. The SERS requirement of roughened surfaces, primarily of the group IB metals, however, has limited (perhaps unduly so[4]) its scope of chemical applications. While infrared reflection-absorption spectroscopy (IRAS) does not exhibit the surface selectivity of SERS, and is more restricted in the range of adsorbates (and vibrational frequencies) that can be examined, it offers the substantial advantage of being applicable to a wide variety of surfaces, including oriented monocrystalline metals. The deleterious influence of solution-phase absorption can be minimized by the use of thin-layer electrochemical cells combined with potential-difference infrared techniques.[3]

Most electrochemical applications of IRAS so far have involved polycrystalline metal surfaces, reflecting in part the traditional interests of surface electrochemists. The fundamental virtues of examining oriented single-crystal surfaces, however, have long been recognized, especially since the fabrication and characterization of monocrystalline metal interfaces is commonplace in uhv surface science. An impediment to the use of such well-ordered surfaces in electrochemical systems was initially the lack of reliable procedures for preparing them in ambient laboratory environments. One approach involves pretreating ordered surfaces instead in uhv, followed by transfer to the electrochemical cell.[1] An important development was the demonstration by Clavilier et al. that ordered low-index platinum faces could be prepared by annealing an appropriately oriented crystal in an air-hydrogen flame, followed by rapid transfer to the electrochemical cell.[5] Although initially controversial, this and related methods are now well-accepted means[6] of preparing well-ordered metal surfaces for in situ electrochemical purposes. One interesting variant developed for platinum and rhodium by Wieckowski and co-workers[7] involves cooling the crystal in an inert gas stream over iodine. The protective iodine monolayer is replaced by CO electrosorption, which can be removed subsequently by voltammetric oxidation. The

† Present address: Dow Chemical Co., Midland, MI 48674.

(1) See for example: (a) Hubbard, A. T. *Chem. Rev.* **1988**, *88*, 633. (b) Kolb, D. M. *Z. Phys. Chem. (Munich)* **1987**, *154*, 179.

(2) For recent reviews, see for example: (a) Weitz, D. A.; Moskovits, M.; Creighton, J. A. In *Chemistry and Structure at Interfaces—New Laser and Optical Techniques*; Hall, R. B., Ellis, A. G., Eds.; VCH Publishers: Deerfield Beach, FL, 1986; Chapter 5. (b) Hester, R. E. In *Comprehensive Chemical Kinetics*; Compton, R. G., Hamnett, A., Eds.; Elsevier: Amsterdam, 1989; Vol. 29, Chapter 2.

(3) For recent reviews, see for example: (a) Bewick, A.; Pons, S. In *Advances in Infrared and Raman Spectroscopy*; Clark, R. J. H., Hester, R. E., Eds.; Wiley: New York, 1985; Vol. 12, Chapter 1. (b) Christensen, P. A.; Hamnett, A. In ref 2b, Chapter 1.

(4) Weaver, M. J.; Corrigan, D. S.; Gao, P.; Gosztola, D.; Leung, L.-W. H. *ACS Symp. Ser.* **1988**, *No. 378*, 303.

(5) (a) Clavilier, J.; Faure, R.; Guinet, G.; Durand, R. *J. Electroanal. Chem.* **1980**, *107*, 205. (b) Also see: Clavilier, J. *ACS Symp. Ser.* **1988**, *No. 378*, 202.

(6) (a) Wagner, F. T.; Ross, P. N., Jr. *J. Electroanal. Chem.* **1988**, *250*, 301. (b) Ross, P. N., Jr. *ACS Symp. Ser.* **1988**, *No. 378*, 37.

(7) (a) Zurawski, D.; Rice, L.; Hourani, M.; Wieckowski, A. *J. Electroanal. Chem.* **1987**, *230*, 221. (b) Hourani, M.; Wieckowski, A. *J. Electroanal. Chem.* **1987**, *227*, 259.

0022-3654/91/2095-5391$02.50/0

long-range surface order produced in this fashion is evident from atomic resolution scanning tunneling microscopy.[8] Flame annealing, as well as electrochemical polishing, procedures have also been utilized to prepare ordered monocrystalline gold and silver electrodes.[9]

These combined developments have led to the recent emergence of infrared spectroscopy as a viable in situ tool for examining adsorption at monocrystalline metal–aqueous interfaces.[10-23] The adsorption of carbon monoxide has been emphasized, although not exclusively so, for several reasons.[10,11,13-22] Besides the large dynamic dipole of the C–O vibration, enabling ready infrared detection even of low CO coverages, the ν_{CO} frequency is especially sensitive to the surface coordination geometry and local environment. In addition, adsorbed CO formed by dissociative chemisorption of organic molecules constitutes a common inhibitor (and possibly also a reaction intermediate) for their electrooxidation on transition-metal surfaces in aqueous media.[24] Most importantly for the present purposes, extensive surface vibrational data obtained by means of both infrared and electron energy loss spectroscopies (EELS) are now available for CO on a number of monocrystalline transition metals in uhv. Given the sensitivity of the CO vibrational features to the chemical and electrostatic environment, detailed intercomparisons of spectra for related metal–solution and metal–uhv systems can be anticipated to yield important new insight into the additional features that characterize the former type of metal interface. Simply stated, the surface chemist is offered for the first time the intriguing prospect of a common vibrational spectroscopic technique being available for the exploration of adsorbate binding on ordered monocrystalline surfaces in both electrochemical and uhv environments.

Discussed herein is the utilization for this purpose of recent infrared spectral data, gathered largely for CO on low-index platinum and rhodium electrodes in our laboratory. Of particular interest is the effect of the electrochemical double layer on the ν_{CO} frequencies and CO coordination geometry. The relationship between these results and related spectral data for metal–uhv systems, particularly involving the electrostatic field effects and solvent coadsorption, is explored along with the predictions of contemporary theoretical models. Such comparisons serve to highlight the virtues of electrochemical systems for unraveling the roles of surface potential (and electrostatic field) on adsorbate binding. The primary overall objective is to demonstrate the value of such experimental spectroscopic links for the development of a unified understanding of fundamental issues common to electrochemical and uhv surface science.

Surface Potential Effects in Electrochemical versus UHV Systems

A unique feature of electrochemical systems is the ability to vary externally the metal–solution potential difference, ϕ_s^M. Besides controlling the occurrence of faradaic (redox) processes, this enables the electrostatic and chemical environment of adsorbed species to be altered in a continuous and systematic fashion. At metal–uhv interfaces, on the other hand, the interfacial potential ϕ_v^M (denoted experimentally by the work function $\Phi^M = e\phi_v^M$) is predetermined by the chemical and physical properties of the system: the bulk metal, the surface crystallographic orientation, and the adlayer composition.

For "perfectly polarizable" electrochemical interfaces, i.e., where faradaic (electron-transfer) processes are entirely absent, the surface electronic charge density σ^M can in principle be deduced as a function of the metal potential, E^M, versus a reference electrode. The potential of zero charge, E_{pzc}^M, where $\sigma^M = 0$, is of particular interest,[25] in part because this electrical state corresponds to that commonly encountered at metal–uhv interfaces in the absence of ionizable adsorbates.[25b] While σ^M–E^M information can be obtained for some monocrystalline metal electrodes, especially gold and silver,[9] it is largely unavailable for transition-metal surfaces, at least in aqueous media, due to the preponderance of adsorbate faradaic processes, especially involving the formation of adsorbed hydrogen and oxide species.[5b] Consequently, E_{pzc}^M values are not known reliably for many electrochemical interfaces, including the systems considered below. Unlike metal–uhv interfaces, then, for which the surface charge σ^M is commonly held at zero, electrochemical interfaces are controlled by the applied electrode potential.

It is therefore valuable to establish a connection between the "surface potentials" E^M and ϕ_v^M that characterize a given metal interface in electrochemical and uhv environments, respectively, in either the presence or absence of adsorbates such as CO. Following Trasatti, a useful relationship for this purpose is[26,27]

$$E^M - \phi_v^M = \delta\chi^M - g^s(\text{dip}) + g_s^M(\text{ion}) + \chi_s - E_K(\text{ref}) \quad (1)$$

Here $\delta\chi^M$ is the change in the "surface electronic" (electron spillover) part of the work function as the metal is contacted with solution, $g^s(\text{dip})$ and $g_s^M(\text{ion})$ are the contributions of solvent dipoles and free charges (ions) to the metal–solution potential drop, χ_s is the surface potential of the solution–vacuum interface, and the "absolute" potential of the reference electrode, $E_K(\text{ref})$, converts the electrode potential E^M to the vacuum reference scale appropriate for ϕ_v^M. The first three terms on the right-hand side of eq 1 enunciate the changes in surface potential that can result from the presence of the electrochemical "double layer".[26] The $g_s^M(\text{ion})$ term can be associated with ionic charge in direct contact with the metal surface (so-called specific adsorption) as well as charge present in the diffuse (outer) part of the double layer. In the particular case where $\sigma^M = 0$ (i.e., $E^M = E_{pzc}^M$) and in the absence of specific ionic adsorption, then $g_s^M(\text{ion}) = 0$.

(8) (a) Schardt, B. C.; Yau, S.-L.; Rinaldi, F. *Science* **1989**, *243*, 1050. (b) Yau, S.-L.; Vitus, C. M.; Schardt, B. C. *J. Am. Chem. Soc.* **1990**, *112*, 3677.

(9) Hamelin, A. In *Modern Aspects of Electrochemistry*; Conway, B. E., White, R. E., Bockris, J. O'M., Eds.; Plenum Press: New York, 1986; Vol. 16, Chapter 1.

(10) (a) Kitamura, F.; Takeda, M.; Takahashi, M.; Ito, M. *Chem. Phys. Lett.* **1987**, *143*, 318. (b) Kitamura, F.; Takahashi, M.; Ito, M. *J. Phys. Chem.* **1988**, *92*, 3320. (c) Kitamura, F.; Takahashi, M.; Ito, M. *Surf. Sci.* **1989**, *223*, 493.

(11) Kitamura, F.; Takahashi, M.; Ito, M. *Surf. Sci.* **1989**, *223*, 493.

(12) Corrigan, D. S.; Brandt, E. S.; Weaver, M. J. *J. Electroanal. Chem.* **1987**, *235*, 327.

(13) Furuya, N.; Motoo, S.; Kunimatsu, K. *J. Electroanal. Chem.* **1988**, *239*, 347.

(14) (a) Juanto, S.; Beden, B.; Hahn, F.; Leger, J.-M.; Lamy, C. *J. Electroanal. Chem.* **1987**, *237*, 119. (b) Beden, B.; Juanto, S.; Leger, J.-M.; Lamy, C. *J. Electroanal. Chem.* **1987**, *238*, 323. (c) Sun, S. C.; Clavilier, J.; Bewick, A. *J. Electroanal. Chem.* **1988**, *240*, 147.

(15) (a) Leung, L.-W. H.; Wieckowski, A.; Weaver, M. J. *J. Phys. Chem.* **1988**, *92*, 6985. (b) Chang, S.-C.; Leung, L.-W. H.; Weaver, M. J. *J. Phys. Chem.* **1989**, *93*, 5341.

(16) (a) Chang, S.-C.; Weaver, M. J. *J. Chem. Phys.* **1990**, *92*, 4582. (b) Chang, S.-C.; Weaver, M. J. *J. Phys. Chem.* **1990**, *94*, 5095. (c) Chang, S.-C.; Weaver, M. J. *Surf. Sci.* **1990**, *230*, 222. (d) Roth, J. D.; Chang, S.-C.; Weaver, M. J. *J. Electroanal. Chem.* **1990**, *288*, 255. (e) Chang, S.-C.; Roth, J. D.; Weaver, M. J. *Surf. Sci.* **1991**, *244*, 113.

(17) (a) Leung, L.-W. H.; Chang, S.-C.; Weaver, M. J. *J. Chem. Phys.* **1989**, *90*, 7426. (b) Chang, S.-C.; Weaver, M. J. *J. Electroanal. Chem.* **1990**, *285*, 263.

(18) (a) Chang, S.-C.; Weaver, M. J. *Surf. Sci.* **1990**, *238*, 142. (b) Chang, S.-C.; Roth, J. D.; Ho, Y.; Weaver, M. J. *J. Electron Spectrosc. Relat. Phenom.* **1990**, *54/55*, 1185.

(19) Chang, S.-C.; Weaver, M. J. *Surf. Sci.* **1991**, *241*, 11.

(20) Jiang, X.; Chang, S.-C.; Weaver, M. J. *J. Phys. Chem.*, in press.

(21) (a) Chang, S.-C.; Hamelin, A.; Weaver, M. J. *Surf. Sci.* **1990**, *239*, L543. (b) Chang, S.-C.; Hamelin, A.; Weaver, M. J. *J. Phys. Chem.*, in press.

(22) (a) Leung, L.-W. H.; Chang, S.-C.; Weaver, M. J. *J. Electroanal. Chem.* **1989**, *266*, 317. (b) Leung, L.-W. H.; Weaver, M. J. *J. Phys. Chem.* **1989**, *93*, 7218. (c) Chang, S.-C.; Leung, L.-W. H.; Weaver, M. J. *J. Phys. Chem.* **1990**, *94*, 6013.

(23) Faguy, P. W.; Markovic, N.; Adzic, R. R.; Fierro, C. A.; Yeager, E. B. *J. Electroanal. Chem.* **1990**, *289*, 245.

(24) For a review, see: Parsons, R.; Vandernoot, T. *J. Electroanal. Chem.* **1988**, *257*, 9.

(25) For example, see: (a) Frumkin, A. N.; Petrii, O. A.; Damaskin, B. B. In *Comprehensive Treatise of Electrochemistry*; Vol. 1, Bockris, J. O'M., Conway, B. E., Yeager, E., Eds.; Plenum: New York, 1980; Chapter 5. (b) Trasatti, S, In *Advances in Electrochemistry and Electrochemical Engineering*; Gerischer, H., Tobias, C. W., Eds.; Wiley: New York, 1977; Vol. 10, p 213.

(26) Trasatti, S. *J. Electroanal. Chem.* **1983**, *150*, 1 and preceding references quoted therein.

Such $E^M_{pcz} - \phi^M_v$ relations have been used to provide estimates of the surface solvent dipole potential g^s(dip).[26] Often, however, g^s(dip) and g^M_s(ion) are not known separately and in any case are both dependent on the electrode potential (vide infra). Most simply, for the present purposes we can define an electrode potential E^M_0 given by

$$E^M_0 = \phi^M_v - E_K(\text{ref}) \quad (2)$$

At the electrode potential E^M_0, the solvent dipolar [g^s(dip)] and "free charge" [g^M_s(ion)] contributions to E^M "nullify" each other, so that the overall potential drop across the electrochemical and uhv interfaces is the same, save for the residual $\delta\chi^M$ and χ_s terms which result from the presence of solvent (rather than vacuum) on the nonmetallic side of the former interface.[15b,16a] Under some circumstances, such as in the presence of a saturated CO adlayer, the solvent dipolar contribution may well be small ($\lesssim$0.1 V) so that E^M_0 as deduced from eq 2 by using metal–uhv data will be close to E^M_{pzc}. (This should especially be the case if the work function data refer to metal–uhv interfaces in the presence of codosed solvent as well as the adsorbate of interest. Such measurements, however, are rare and usually refer to low temperatures ($\lesssim$150 K) so to avoid solvent desorption; vide infra.) In any case, provided that the effect of g^s(dip) upon the field sensed by the adsorbate is not greatly different from that of the free charges, this comparison between E^M_0 and ϕ^M_v is approximately valid even if g^s(dip) $\neq$ 0. As a starting point, then, it is profitable to compare the spectroscopic properties of CO (and other uncharged molecular adsorbates) at a given metal–solution interface held at an electrode potential E^M_0 that corresponds (via eq 2) to the work function $e\phi^M$ of the corresponding metal–uhv surface containing the same CO coverage.[15b]

There is also some uncertainty in the appropriate value of E_K(ref). While a value of about 4.45 V for E_K(ref) of a normal hydrogen electrode (NHE) has been deduced from thermodynamic arguments,[26,27] estimates around 4.7–4.8 V have been extracted on the basis of work function measurements for electrode surfaces transferred into uhv[28] and by other means.[29] While arguments favoring the latter estimate have become prominent of late,[30] the issue remains in essence unresolved at the present time. We will utilize here an "average" estimate, 4.6 V, of E_K(ref) for the NHE. Fortunately, for the present illustrative purposes these uncertainties in E_K(ref) are relatively inconsequential.

Influence of the Electrode Potential on CO Chemisorption

Potential–Vibrational Frequency Dependencies. A commonly observed, yet striking, characteristic of metal–solution interfaces is that the vibrational frequencies of adsorbed molecules depend significantly on the electrode potential.[31] These dependencies can arise in part from variations in adsorbate coverage and binding site geometry.[16d] Of primary interest, however, is the frequency–potential (ν–E) dependencies at *fixed* adsorbate coverage and site occupancy. This effect, while often termed "Stark tuning", may arise from potential-dependent surface bonding[32] as well as from electrostatic field (first-order Stark) phenomena.[33] A similar effect has also been observed at metal–uhv interfaces by modulating the local electrostatic field.[33]

Of fundamental interest is the evaluation of such ν–E dependencies as a function of the surface crystallographic structure and the adsorbate coverage and binding geometry. Besides affording a direct comparison with (and a test of) these theoretical models, such information is necessary in order to compare the adsorbate vibrational properties for corresponding metal–solution and metal–uhv interfaces at equivalent potentials (see below). Contained in Table I are representative ν_{CO}–E slopes for CO bound in terminal (i.e., atop) and bridging configurations, $d\nu^t_{CO}/dE$ and $d\nu^b_{CO}/dE$, respectively, on low-index platinum and rhodium surfaces in aqueous 0.1 M $HClO_4$. These data, taken from a more extensive tabulation in ref 18a, refer to conditions where the adsorbate site occupancy, as gleaned from the band absorbance, does not vary significantly with electrode potential. (This condition is necessary to avoid contributions to $d\nu_{CO}/dE$ from variable adsorbate dipole–dipole coupling and other coverage-dependent environmental effects.[31]) It should be noted that the data for subsaturated CO coverages in Table I, and elsewhere in the present work, refer to adlayers formed by exposure to dilute CO solutions.[18a] The nature of such "dosed" adlayers differs substantially from those formed by partial electrooxidative removal of a saturated CO layer.[16,35]

TABLE I: Representative Infrared ν_{CO} Frequency–Potential Slopes for CO Adsorbed in Terminal and Bridging Geometries at Monocrystalline Pt- and Rh–Aqueous Interfaces[a]

surface	potential vs NHE, V	θ_{CO}[b]	ν^t_{CO},[c] cm^{-1}	$d\nu^t_{CO}/dE$,[d] cm^{-1} V^{-1}	ν^b_{CO},[e] cm^{-1}	$d\nu^b_{CO}/dE$,[f] cm^{-1} V^{-1}
Pt(111)	0.1	≈0.65	2062	32	1776	58
	0.55	≈0.65	2072	25	1844	46
	0.25	0.3	2055	40	1836	40
	0.25	0.13	2047	43		
	uhv[g]	≈0.6		(≈10)[g]		(~15)[g]
		≈0.05		(≈16)[g]		
Pt(100)	0.25	0.85	2057	36		
Pt(110)	0.05	1.0	2069	32		
Rh(111)	0.25	0.75	2034	30	1805	47
Rh(100)	0.25	0.75	2021	34	1933	37
	0.25	0.25			1861	57

[a] Data taken from ref 18a, unless stated otherwise; electrolyte was 0.1 M $HClO_4$ in each case. [b] Fractional CO coverage (i.e., number of adsorbed CO molecules per surface metal atom). [c] Peak frequency of terminal ν_{CO} band at electrode potential and CO coverage indicated. [d] Frequency–potential slope of terminal ν_{CO} band for potential and coverage conditions indicated. (Reliability is ca. ±2–5 cm^{-1} V^{-1}.) [e] Peak frequency of bridging ν_{CO} band for conditions indicated. [f] Frequency–potential slope of 2-fold (or 3-fold) bridging ν_{CO} band for conditions indicated. (Reliability is ca. ±2–5 cm^{-1}.) [g] Values refer to Pt(111)–uhv interface. Extracted from ν_{CO} frequency–local electrostatic field slopes quoted in ref 34a (and for θ_{CO} ~0.05 from ref 34b) by assuming that "thickness" of CO adlayer is 3.5 Å (see text).

At least two trends are evident in Table I, which are also observed more generally.[18a] First, while the $d\nu_{CO}/dE$ values lie mostly in the range ca. 30–60 cm^{-1} V^{-1}, they tend to increase toward lower CO coverages, θ_{CO}. Second, the $d\nu_{CO}/dE$ values are larger for bridging than for terminal coordinated CO. In addition, there is evidence that the $d\nu_{CO}/dE$ slopes decrease progressively toward more positive potentials in some cases.[31] This ν_{CO}–E nonlinearity is seen most clearly for CO on Pt(110), for which $d\nu^t_{CO}/dE$ diminishes from ca. 35 to 20 cm^{-1} V^{-1} over the accessible (≈0.8 V) potential range.[31] This system exhibits almost exclusively terminal binding, thereby eliminating complications from potential-induced changes in site occupancy.[16c]

Interestingly, related data have been reported recently for CO on Pt(111) in uhv.[34] The procedure in essence entails evaluating the ν_{CO} frequency changes in response to a modulating electric field applied between the surfaces of interest and a nearby elec-

(27) Note that ϕ^M is defined here as a potential, rather than as an energy; the work function is usually given in energy units (eV) and therefore is equal to $e\phi^M$, where e is the electronic charge.
(28) Kötz, R.; Neff, H.; Müller, K. *J. Electroanal. Chem.* **1986**, *215*, 331.
(29) Gomer, R.; Tryson, G. *J. Chem. Phys.* **1977**, *66*, 4413.
(30) For example, see: Hansen, W. N.; Hansen, G. J. *ACS Symp. Ser.* **1988**, *No. 378*, 166.
(31) Earlier examples for polycrystalline surfaces include: (a) Bewick, A.; Kunimatsu, K.; Robinson, J.; Russell, J. W. *J. Electroanal. Chem.* **1981**, *119*, 175. (b) Kötz, R.; Yeager, E. *J. Electroanal. Chem.* **1981**, *123*, 335.
(32) Anderson, A. B. *J. Electroanal. Chem.* **1990**, *280*, 37.
(33) Lambert, D. K. *J. Chem. Phys.* **1988**, *89*, 3847 and previous references cited therein.
(34) (a) Luo, J.-S.; Tobin, R. G.; Lambert, D. K.; Wagner, F. T.; Moylan, T. E. *J. Electron Spectrosc. Relat. Phenom.* **1990**, *54/55*, 469. (b) Lambert, D. K. Personal communication.
(35) Adlayers formed by partial electrooxidative stripping typically exhibit ν_{CO} frequencies and relative band intensities for differing coordination geometries that are nearly invariant with coverage.[16-18] This behavior is indicative of the presence of large CO domains ("islands") having high local coverages, formed as a result of CO electrooxidation to CO_2 occurring only at island edges, where the oxident (water or hydroxyl) can coadsorb in an adjacent site.[16e]

trode.[33] The fields involved, ca. 3×10^4 V cm^{-1}, are much smaller than those commonly encountered at metal–electrolyte interfaces. In the latter systems, virtually the entire potential difference occurs within the double layer; for high electrolyte concentrations this potential drop is confined largely within the inner layer [i.e., between the charged metal surface and the so-called outer Helmholtz plane (oHp), where the ionic countercharge primarily resides]. A reasonable estimate of this inner-layer thickness for the present systems[33] is 3.5 Å; a 1-V potential drop, for example, then corresponds to an inner-layer field of 3×10^7 V cm^{-1}.

Included in Table I are $d\nu_{CO}/dE$ estimates for terminal and bridging CO at the Pt(111)–uhv interface. These were extracted from the corresponding ν_{CO} frequency–electrostatic field slopes in ref 34 by assuming that the "thickness" of the CO adlayer is 3.5 Å, thereby converting these data into units common to the electrochemical results.[36] (The converse, yet essentially equivalent, procedure was employed in ref 34; i.e., the electrochemical $d\nu_{CO}/dE$ data were converted into frequency–field slopes by assuming an inner-layer thickness of 3.5 Å.)

Comparison of the corresponding $d\nu_{CO}/dE$ values for Pt(111)/CO ($\theta_{CO} \sim 0.6$) in aqueous electrochemical and uhv environments (Table I) shows that the latter are ca. 3-fold smaller, for both terminal and bridge-bound CO. Aside from the uncertainties involved in the conversion from field to potential units, this discrepancy may reflect an influence of the solvent and ions in the electrochemical system. However, as discussed below, the electrochemical $d\nu_{CO}/dE$ values refer to substantially (ca. 1.0 V) less positive surface potentials (on the vacuum scale). Given that the electrochemical $d\nu_{CO}/dE$ values can diminish toward more positive potentials (vide supra), the smaller values observed in uhv may be rationalized at least semiquantitatively on this basis. Another plausible explanation is that externally applied electric field is screened to a greater extent at the Pt(111)–uhv than at the electrochemical interface.[34b] Nevertheless, in addition to the larger $d\nu_{CO}/dE$ values for bridging versus terminal CO, both the Pt(111)–uhv and electrochemical surfaces display roughly comparable decreases in $d\nu_{CO}/dE$ with increasing θ_{CO} (Table I). The latter effect may well be due to screening of the local electric field by nearby CO adsorbate.

As already mentioned, such ν_{CO}–E data when placed on an appropriate reference potential scale can be utilized to provide a comparison of the band frequencies in corresponding electrochemical and uhv environments.[15b,18b] Examples of this procedure applied to terminal coordinated CO in saturated adlayers on Pt(111), Pt(100), Pt(110), and Rh(111) are illustrated in Figure 1. These systems were selected because the coordination geometries, at least with regard to the relative terminal/bridging site occupancy, do not differ markedly between the electrochemical (aqueous 0.1 M $HClO_4$) and uhv environments. The continuous solid lines in Figure 1 represent the electrochemical ν^t_{CO}–potential data; the positive limit in each case corresponds to the onset of CO electrooxidation. The filled symbols refer to the ν^t_{CO} and ϕ^M values obtained for the corresponding metal–uhv system. (See refs 16–18 for data sources.) The x-axis potential scale, ϕ^M (V), is defined by eq 2; i.e., the electrochemical potentials are quoted on the vacuum rather than the NHE scale.

Noteworthy are the substantially (ca. 0.5–1.5 V) more positive potentials (i.e., higher work functions) that characterize the *uncharged* anhydrous metal–uhv interfaces. The lower potentials for the electrochemical systems arise from the presence of negative surface electronic charges, possibly along with preferential water dipole orientation [g^M_s(ion) and g^s(dip), respectively, in eq 1]. The dashed lines constitute extrapolations of the electrochemical results to potentials appropriate for the corresponding uhv interfaces. For Pt(111), Pt(100), and Rh(111), this analysis indicates that the lower ν^t_{CO} values that are observed in the electrochemical versus uhv environments arise primarily from the less positive potentials

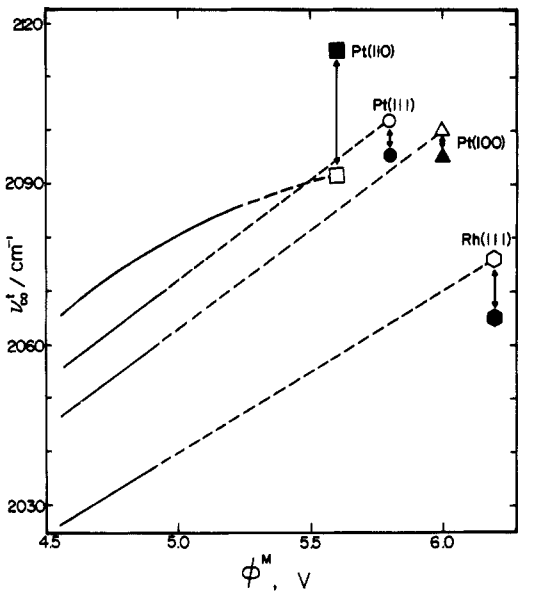

Figure 1. Comparison of extrapolated ν_{CO} frequency–electrode potential plots at fixed adsorbate site occupancy for terminal coordinated CO (at saturated θ_{CO} values) at metal–aqueous interfaces (solid lines) with ν_{CO} values for corresponding metal–uhv systems, on a common surface potential scale, ϕ^M (versus vacuum), for four surfaces, as indicated. The filled symbols are metal–uhv data plotted at the ϕ^M values obtained from work function data for the metal/CO uhv interface (see refs 16 and 17a for details); the open symbols are the corresponding electrochemical data extrapolated to the same ϕ^M values. The solid lines represent best fits to at least 10 data points for each system. See text and ref 18a for further details.

that characterize the former interfaces. Indeed, the extrapolations can yield even closer consistency if ν^t_{CO}–E nonlinearities, as noted above, are considered. This ν^t_{CO}–E curvature is pictured in Figure 1 for the most definitive example, Pt(110); essentially linear extrapolated ν_{CO}–E plots are given for the other surfaces for simplicity even though there is evidence, such as for Pt(111),[16d] that significant nonlinearities are present on a more general basis. The Pt(110)/CO system, however, does not yield satisfactory agreement between the extrapolated electrochemical and uhv ν^t_{CO} values (Figure 1). (See ref 16c for a discussion of this point.) We stress here that Figure 1 is meant for illustrative and not quantitative purposes; subtle differences in the CO adlayer structure between the electrochemical and uhv environments, as well as uncertainties in E_K(ref) and the uhv ϕ^M values (both ca. 0.1–0.2 V), preclude a more precise comparison.

The significant positive potential extrapolations that are necessary to compare the ν_{CO} frequencies in electrochemical and uhv surface environments can be circumvented by employing nonaqueous media so as to avoid the occurrence of CO electrooxidation. Recent ν_{CO}–E data for saturated CO layers on Pt(111) in several nonaqueous solvents yield ν^t_{CO} values, ca. 2090–2095 cm^{-1}, at electrode potentials equivalent to the Pt(111)/CO–uhv interface that are close to the measured value, ca. 2095 cm^{-1}, for the latter system.[37]

Of central interest is the comparison of such ν_{CO} frequency–potential data with the predictions of contemporary theoretical models. Variations in electrode potential may be expected to influence adsorbate frequencies, both as a consequence of changes in the local electrostatic field (Stark effect) and from alterations in the adsorbate–metal bonding. Both these types of effects have recently been considered in detail.[32,33,38–43] The first-order Stark

(36) This procedure is, of course, artificial since the electrostatic field extends far beyond the adsorbate layer in the metal–UHV system.

(37) Chang, S.-C.; Jiang, X.; Roth, J. D.; Weaver, M. J. *J. Phys. Chem.*, in press.

(38) Holloway, S.; Norskov, J. K. *J. Electroanal. Chem.* **1984**, *161*, 193.
(39) Korzeniewski, C.; Pons, S.; Schmidt, P. P.; Severson, M. W. *J. Chem. Phys.* **1986**, *85*, 4153.
(40) Anderson, A. B.; Kötz, R.; Yeager, E. *Chem. Phys. Lett.* **1981**, *82*, 130.
(41) Mehandru, S. P.; Anderson, A. B. *J. Phys. Chem.* **1989**, *93*, 2044.
(42) Philpott, M. R.; Bagus, P. S.; Nelin, C. J.; Seki, H. *J. Electron Spectrosc. Relat. Phenom.* **1987**, *45*, 169.
(43) Bagus, P. S.; Pacchioni, G. *Surf. Sci.* **1990**, *236*, 233.

effect, resulting from a rigid dipole oscillator in a variable electric field, is conceptually a straightforward (and inevitable) component of the observed frequency shifts. Lambert has provided the most detailed discussion; at least semiquantitative agreement with the experimental ν_{CO}–E slopes can be obtained in some cases.[33] However, the first-order Stark effect *by itself* does not provide a ready explanation of the observed nonlinearities in the ν_{CO}–E plots or the higher $d\nu_{CO}/dE$ slopes found for bridging versus terminal CO. The former observation might be accounted for by including field-induced dipolar effects (higher order Stark terms). Indeed, consideration of polarizability factors can rationalize the observed potential dependence of the CO infrared band absorbance in the Pt(110)/CO and other systems.[44]

The role of adsorbate–metal bonding in describing the ν_{CO}–E behavior has also been considered. Anderson has developed a semiempirical bonding approach, labeled the "atom superposition and electron delocalization molecular orbital" (ASED-MO) theory.[32,40,41,45] In essence, this treatment is based on a physical model that involves partitioning the molecular and electronic charge distribution functions for an appropriate model cluster into "rigid atomic" and "delocalized" components, which yield repulsive and attractive potential energy contributions, respectively. Alteration of the electrode potential is mimicked by varying the valence-state ionization potential of the metal cluster atoms and hence the metal surface electronic energy.[32,45] Such energetic alterations affect the degree of adsorbate–surface orbital mixing.

In the case of CO, shifting the potential to less positive values increases the extent of metal–adsorbate $d\pi$–$2\pi^*$ back-donation; in the ASED-MO model this effect is primarily responsible for the predicted decreases in ν_{CO} as the potential is lowered. (The greater extent of such back-donation for bridging relative to terminal CO coordination is also reflected in the lower ν_{CO} frequencies characteristic of the former binding geometry; Table I.) Interestingly, the ASED-MO model predicts $d\nu_{CO}/dE$ values for CO at different coordination geometries in the following sequence: terminal < 2-fold < 3-fold site, resulting from the greater potential-dependent degree of $d\pi$–$2\pi^*$ back-bonding engendered by multiple-site coordination. This prediction is in qualitative accord with experiment (Table I).

Such observed dependencies of the $d\nu_{CO}/dE$ values on the adsorption site geometry are difficult to account for purely on the basis of the electrostatic Stark effect, that is, without considering additionally surface-bonding factors. Bridge-bound CO is known to induce larger work function increases than terminal CO; this has been interpreted in terms of a larger adsorbate dipole moment ($^{\delta+}C{\equiv}O^{\delta-}$) in the former geometry.[46] This enhanced dipole moment most likely arises from greater $d\pi$–$2\pi^*$ back-donation.[47] Given that the magnitude of the first-order Stark effect is proportional to the adsorbate dipole moment, the larger $d\nu_{CO}/dE$ slopes observed in the bridging coordination geometry can therefore be rationalized on this basis, i.e., by including metal–adsorbate charge transfer in the electrostatic picture.

Recently, Bagus et al. have utilized ab initio MO theory to evaluate field-dependent bonding of CO on copper[42] and palladium.[43] In the latter case (for a Pd_2CO model), the degree of $d\pi$–$2\pi^*$ back-bonding is predicted not to vary substantially with potential, such that the major contribution to the ν_{CO}–E dependence is asserted to arise from an electrostatic Stark effect.[43] However, the electrode potential variation is modeled entirely in this case by applying an electrostatic field across the cluster, rather than by altering the surface electronic energy, as in the ASED-MO model. While both approaches have their merits, the latter tactic might be expected to provide a more appropriate description of electrochemical potential effects upon adsorbate–surface bonding.

Potential-Dependent Binding Site Geometries. In addition to the striking effects of altering the electrode potential on adsorbate vibrational frequencies, marked changes can occur in the adsorbate coordinatiion geometry. Such effects are readily discerned for CO in view of the well-known sensitivity of the ν_{CO} frequency to the nature of the surface binding site (Table I). In this manner, dramatic potential-induced changes in site occupancy are observed for CO on several low-index platinum and rhodium surfaces. An example is illustrated in Figure 2, which consists of a potential-dependent sequence of ν_{CO} spectra for a saturated CO coverage (θ_{CO} = 0.75) on Rh(111) in 0.1 M $NaClO_4$. The spectra were acquired during a slow (1 mV s^{-1}) positive-going potential sweep.[18a] Twofold bridging coordination dominates at the most negative potentials, as discerned from a band at ca. 1885 cm^{-1}. As the potential is shifted beyond 0 V, this band is replaced entirely by a terminal feature, at 2020–2030 cm^{-1}. Qualitatively similar potential-induced site conversion at high θ_{CO}, favoring increasingly bridging CO coordination at lower potentials, has also been observed on Pt(111),[10c,18a] Pt(100),[10a,b,16b] and Rh(100).[18a] Related effects are also obtained at lower CO coverages but are more susceptible to the additional influence of solvent and/or hydrogen coadsorption (vide infra).

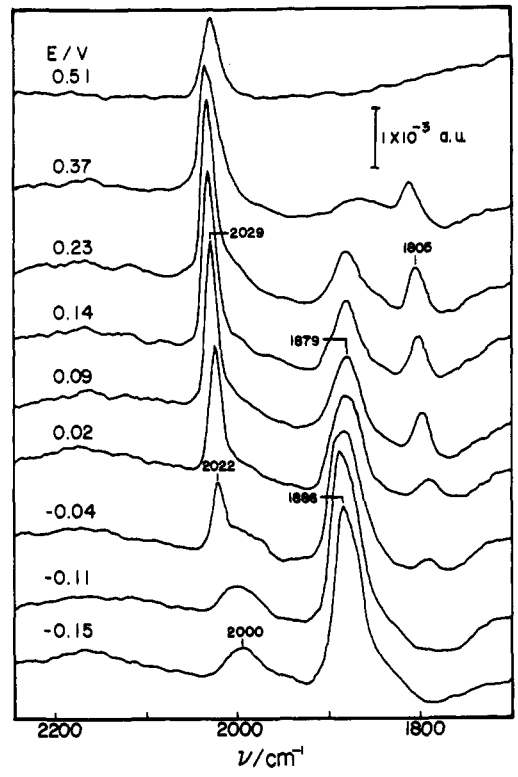

Figure 2. Sequence of infrared absorbance spectra in the 1700–2200 cm^{-1} region for irreversibly adsorbed CO (θ_{CO} = 0.75) on Rh(111) in aqueous 0.1 M $NaClO_4$ obtained during positive-going potential sweep (1 mV s^{-1}) from −0.15 V vs NHE. Potentials shown are average values during spectral data acquisitions; this involved acquiring sets of 100 interferometer scans, subtracted from which was a similar set obtained following complete CO electrooxidation (see ref 18a for further details).

These potential-dependent site occupancies are illustrated in more quantitative fashion in Figure 3, which is a plot of the fraction of the total integrated absorbance due to the terminal ν_{CO} band (A_t/A_{tot}) at near-saturated θ_{CO} values against the electrode potential on the vacuum scale, ϕ^M, for Pt(111), Pt(100), Rh(111), and Rh(100), as indicated. The solid traces refer to the electrochemically accessible potential ranges, limited by CO electrooxidation and hydrogen evolution. The data utilized for Figure 3, taken partly from Table 2 of ref 18a, were obtained in alkaline as well as acidic aqueous media so to expand the accessible range of electrode potentials bordered by these faradaic processes. [Examples of the spectra utilized for this purpose, obtained specifically in 0.1 M $HClO_4$ at 0 V vs NHE, are illustrated in Figure 4 (lower spectra) for all six low-index Pt and Rh surfaces.] Similarly to Figure 1, the symbols plotted in Figure 3 at more positive potentials are the A_t/A_{tot} values for the corresponding

(44) Lambert, D. K. *J. Chem. Phys.* **1991**, *94*, 6237.
(45) Anderson, A. B.; Grimes, R. W.; Hong, S. Y. *J. Phys. Chem.* **1987**, *91*, 4245.
(46) (a) Surnev, L.; Xu, Z.; Yates, J. T. *Surf. Sci.* **1988**, *201*, 14. (b) Mate, C. M.; Kao, C.-T.; Somorjai, G. A. *Surf. Sci.* **1988**, *206*, 145.
(47) Nieuwenhuys, B. E. *Surf. Sci.* **1981**, *105*, 505.

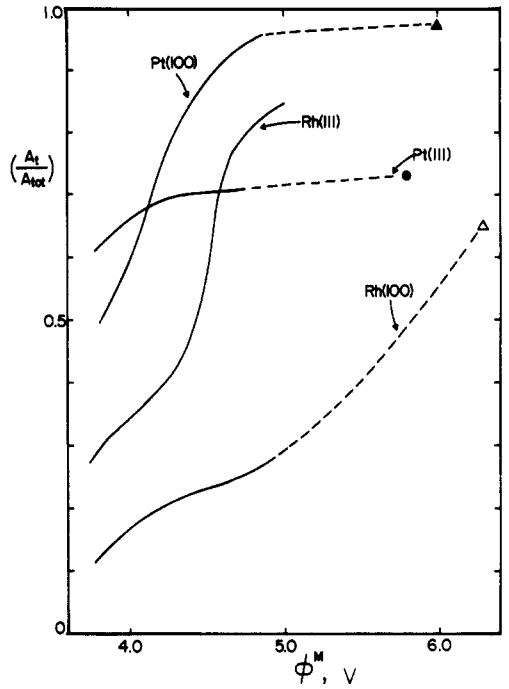

Figure 3. Plot of the ratio of the integrated absorbance for the terminal ν_{CO} band to the total absorbance for all ν_{CO} bands (A_t/A_{tot}) at near-saturated θ_{CO} values against surface potential ϕ^M (on vacuum scale) for four surfaces, as indicated. The solid curves represent potential-dependent data obtained for the metal–aqueous interface, and the symbols are A_t/A_{tot} values for the corresponding metal–uhv interfaces. Absorbance ratios are taken from Table 2 of ref 18a; ϕ^M values for metal–uhv interfaces are from sources as noted in refs 16a,b and 17. Dashed traces represent "best fit" extrapolations between the corresponding electrochemical and uhv data.

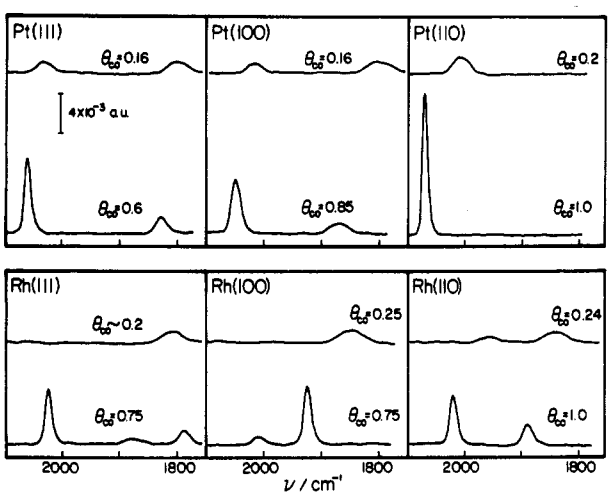

Figure 4. Representative infrared spectra (on common absorbance scale) for CO irreversibly adsorbed on platinum and rhodium low-index surfaces, as indicated, in aqueous 0.1 M $HClO_4$ at 0 V vs NHE, at saturation CO coverages (lower spectra), and low or intermediate coverages (upper spectra), as noted. See ref 18a for further details.

metal–uhv interface. The dashed segments represent a pictorial link between these electrochemical and uhv data. [Note that IRAS data are as yet unavailable for the Rh(111)/CO uhv interface.] These results indicate, at least in semiquantitative fashion, that the observed differences in CO site occupancy in corresponding aqueous electrochemical and uhv systems can again be rationalized in terms of the differing surface potentials between these two types of interfacial environment.

Similar changes in CO site occupancy at near-saturated θ_{CO} values have been induced at metal–uhv interfaces by coadsorption. By using EELS, Somorjai and co-workers observed a complete shift of CO ($\theta_{CO} \sim 0.5$) on Pt(111) from terminal to bridging coordination caused by increasing coverages of preadsorbed potassium.[48a] Similar results have also been observed for the corresponding Rh(111) system.[48b] The adsorption of even low coverages of potassium (and other alkali metals) in the presence or absence of CO lowers the substrate work function substantially (1–2 eV), reflecting marked electron donation to the metal surface.[49] Comparable results have been obtained for the coadsorption of phosphine (PH_3) with CO on Pt(111), for conditions where the former species lowers the work function by ca. 1 eV.[50]

As a consequence, one can envisage such site occupancy changes occurring in an analogous fashion to the potential-induced shifts observed in related electrochemical systems. Indeed, the vibrational spectroscopic data for the Pt(111)/CO,K–uhv interface[48] when combined with corresponding work function measurements[50] yield potential-dependent CO site occupancies, and also ν_{CO} frequencies, which are roughly similar to those for the corresponding electrochemical surface (Figure 3)[18a] when compared on a common potential scale. Such analogies are not expected to be complete, however, since the coadsorbate in uhv may influence the CO bonding via short-range as well as long-range (nonspecific) interactions.[51] The distinction between, and assignment of, these interaction effects has been controversial. For the electrochemical systems, on the other hand, the variation in the interfacial potential drop is brought about primarily by the surface electronic charge balanced by the free ionic countercharge (g_s^M(ion) in eq 1) (also see below). In the absence of specific ionic adsorption (as expected for cations, especially in the presence of adsorbed CO), this countercharge lies within the diffuse (rather than the inner) layer, where its influence upon the adsorbate properties should be nonspecific in origin. Indeed, variation in the nature and concentration of the aqueous electrolyte cation (e.g., H_3O^+, Li^+, K^+, Mg^{2+}, Ba^{2+}, La^{3+}) yields for the most part only minor differences in the form of the ν_{CO} spectra on monocrystalline platinum electrodes, even at relatively negative electrode potentials.[52]

The ASED-MO model of Anderson readily predicts potential-induced site occupancy shifts for electrochemical systems.[41,53] Thus for Pt(111)/CO (mimicked computationally by an appropriate Pt cluster), the terminal coordination is predicted to be favored energetically only at more positive potentials, the 2-fold (and 3-fold) geometries being more stable at lower potentials. Such a theoretical expectation is borne out by the experimental findings.[18a] Physically, this coordination shift can be considered to be triggered by the increased extent of $d\pi$–$2\pi^*$ back-donation occurring at lower potentials (i.e., at more negative surface charges) given that such charge transfer will be more extensive for bridging versus terminal CO coordination.

Of interest is the differing behavior observed experimentally for Rh(100) versus Rh(111), in that the former electrochemical surface exhibits a markedly greater propensity for bridging CO coordination (Figure 3). Recent ASED-MO calculations for these surfaces indicate that indeed 2-fold bridging coordination on Rh(100) is favored throughout the accessible range of potentials in the electrochemical environment.[53a] Terminal bonding approaches comparable stability only at the large positive potentials that are characteristic of the Rh(100)/CO–uhv interface. (Indeed, terminal CO bonding is more prevalent under these conditions; Figure 3.[54]) In contrast, the Rh(111) surface is predicted by ASED-MO to favor terminal coordination except at relatively low potentials [similarly to Pt(111)], again in harmony with the experimental results (Figure 2).[18a] The ASED-MO approach[53b] can

(48) (a) Crowell, J. E.; Garfunkel, E. L.; Somorjai, G. A. *Surf. Sci.* **1982**, *121*, 303. (b) Crowell, J. E.; Somorjai, G. A. *Appl. Surf. Sci.* **1984**, *19*, 73.
(49) Kiskinova, M.; Pirug, G.; Bonzel, H. P. *Surf. Sci.* **1983**, *133*, 321.
(50) Mitchell, G. E.; Henderson, M. A.; White, J. M. *Surf. Sci.* **1987**, *191*, 425.
(51) For example, see: Uram, K. J.; Ng, L.; Yates, J. T. *Surf. Sci.* **1986**, *177*, 253.
(52) Chang, S.-C.; Weaver, M. J. Unpublished results.
(53) (a) Chang, S.-C.; Anderson, A. B.; Weaver, M. J. *J. Phys. Chem.*, submitted for publication. (b) Chang, S.-C.; Weaver, M. J.; Anderson, A. B. Unpublished results.
(54) Leung, L.-W. H.; He, J.-W.; Goodman, D. W. *J. Chem. Phys.* **1990**, *93*, 8328.

also account in global terms for the observed marked differences in potential-dependent CO binding geometry on group VIII metals, the preference for terminal versus bridging coordination diminishing in the sequence Ir(111) < Pt(111) < Rh(111) < Pd(111).[20]

Recently, Yates and co-workers have observed a similar terminal–bridge site occupancy shift for a saturated CO adlayer (θ_{CO} = 0.5) on Ni(111) that is induced by subsequent dosing with a variety of small molecules, including CO_2, NH_3, CH_3Br, and CH_3NH_2, which also are observed to decrease the work function ϕ^M.[55] Significantly, the proportion of terminal CO, as discerned from the A_t/A_{tot} ratio, when plotted against $\Delta\phi^M$ falls on a common curve, independent of the chemical nature of the coadsorbate. Interpretation of these interesting results can be couched in terms of electrostatic field effects.[55] As the work function decreases, the anticipated field caused by the postdosed adsorbate dipoles (together with their images in the metal) should favor increasingly CO coordination in a manner yielding a larger $^{\delta+}C{\equiv}O^{\delta-}$ dipole. The observed shift from terminal to bridging coordination is in harmony with this expectation since, as noted above, the latter geometry features a larger dipole moment resulting from more extensive $d\pi-2\pi^*$ back-donation.

This approach can in principle also account for site occupancy shifts where the surface-potential changes are induced by variations in metal electronic charge, as in electrochemical systems and at metal–uhv interfaces where the inner-layer electrostatic field is altered by coadsorbate charge transfer, as for alkali-metal adsorbates. This "electrostatic field" approach is physically quite distinct from the ASED-MO model in that the latter emphasizes, and predicts, the potential-dependent nature of the surface bonding. Nevertheless, it is important to note that the former model nonetheless *utilizes* the difference in the degree of $d\pi-2\pi^*$ back-bonding between the terminal and bridging geometries, as reflected in the larger $^{\delta+}C{\equiv}O^{\delta-}$ dipole for the latter coordination mode.

It is also appropriate to comment on the relationship of chemisorbate structural shifts at metal–uhv interfaces induced by coadsorbate dipolar fields, as in the Ni(111)/CO example noted above,[55] to the role of the solvent (and other dipolar coadsorbates) at electrochemical interfaces. For such metal–uhv interfaces in the absence of adsorbates that yield extensive charge transfer (such as alkali metals), the surface excess charge density will be essentially zero. For electrochemical interfaces, this situation corresponds to $g_s^M(\text{ion}) = 0$ (eq 1), whereupon E^M will equal the potential of zero charge, E_{pzc}^M. Substantial changes in E^M, and equivalently in the work function, can still occur in the presence of oriented solvent (and other) dipoles, whereupon $g^s(\text{dip}) \neq 0$ (eq 1). Variation in this surface-potential component *alone* is responsible for the Ni(111)/CO site occupancy shifts noted by Yates et al.[55]

Alteration of the potential of *electrochemical* interfaces, however, is induced by varying the electronic surface charge, and hence $g_s^M(\text{ion})$ in eq 1. While variations in $g^s(\text{dip})$ also occur under these conditions, the dipoles will tend to realign so to *oppose* the electrostatic field induced by the free charges. For example, inner-layer water is believed to be aligned preferentially with the oxygen and hydrogens oriented toward the metal surface at large positive and negative electrode charges, respectively.[56] Consequently, then, the free-charge and dipolar components of the metal–solution potential drop will commonly be closely coupled, so to provide partly offsetting contributions to the electronic charge-induced variations in the electrode potential.

Coadsorbate Effects on CO Chemisorption

Water and Hydrogen Coadsorption at Electrochemical Interfaces. So far, we have considered primarily the intercomparison of ν_{CO} spectra obtained in electrochemical and uhv environments at high CO coverages. While this condition may engender complications in the site occupancy from adsorbate packing factors, it has the virtue of minimizing additional influences from coadsorption of solvent, hydrogen, or electrolyte ions in the electrochemical systems. The absence of hydrogen coadsorption, in particular, in the presence of saturated CO adlayers is readily discerned from the nonappearance of voltammetric charging currents associated with formation of adsorbed hydrogen from protons (or water) that are otherwise observed at lower potentials (typically 0.25–0 V vs NHE in strongly acidic media).

The form of the θ_{CO}-dependent infrared spectra on low-index Pt and Rh electrochemical surfaces at a given potential typically differs markedly from that observed for the corresponding uhv interfaces.[16-18] Thus for Pt(111), for example, a 2-fold bridging coordination becomes predominant at low dosed coverages under most electrochemical conditions,[16a,18a] whereas essentially exclusive terminal binding occurs for $\theta_{CO} < 0.3$ in the anhydrous uhv environment.[57] An increasing preference for bridge bonding toward lower θ_{CO} is also observed for the Rh(100), Rh(110), and Pt(100) electrochemical interfaces.[16b,17b,18a] No clear preference for bridge bonding is observed for Rh(100)[54,58] in uhv under these conditions in the absence of coadsorbed water or hydrogen, even though bridge as well as terminal coordination is observed on the unreconstructed (1 × 1) Pt(100) uhv surface at low θ_{CO}.[59]

The differing θ_{CO}-dependent behavior of these electrochemical and uhv systems may again be understood, at least partly, in terms of the greater preference of bridging versus terminal coordination in the former environment resulting from the lower surface potentials. Generally speaking, the differences in site occupancy between corresponding electrochemical and uhv systems are more marked at low compared with high θ_{CO}. This may well be due to the influence of stereochemical adsorbate packing factors in moderating the relative CO site occupancies at near-saturated coverages.

Some evidence, however, indicates that the coadsorbed water and/or hydrogen present in the electrochemical inner layer at lower θ_{CO} values can exert a significant specific influence on the adlayer structure. The first example involves Rh(111). The low-coverage ($\theta_{CO} \sim 0.2$) spectrum shown for this surface in Figure 4 (at 0 V vs NHE in 0.1 M $HClO_4$) exhibits a dominant bridging ν_{CO} feature, contrasting the predominant terminal coordination at high θ_{CO}. While this θ_{CO}-dependent coordination by itself is consistent with that of the other surfaces, altering the electrode potential from 0 to ca. 0.3 V vs NHE yields a complete shift of the bridging CO at low θ_{CO} on Rh(111) to terminal binding.[18a] While such a potential-induced site conversion is qualitatively consistent with the high-θ_{CO} behavior in Figure 3, the corresponding Pt(111) surface retains predominantly bridging CO under these conditions.[16a,18a] Given that rhodium is anticipated, and usually observed, to favor bridge bonding to a greater extent than the corresponding platinum surface at a given potential,[53] such low-θ_{CO} behavior is unexpected. The potential region, 0–0.3 V, where the site conversion occurs on Rh(111) coincides with the replacement of coadsorbed atomic hydrogen by water, implying that one (or both) of these species plays a role in the site conversion process.

The second, perhaps more clear-cut, example involves Pt(100). At high θ_{CO}, altering the potential in the positive direction yields increasingly predominant terminal binding, as expected (Figure 3). At low CO coverages ($\theta_{CO} \lesssim 0.3$) on Pt(100) in 0.1 M $HClO_4$, however, exactly the opposite behavior can be discerned: altering the potential from 0 to 0.25 V vs NHE yields a complete removal of the terminal CO in favor of the 2-fold bridging form.[16b] Since this effect is *qualitatively* different from that otherwise observed (and expected) from potential-dependent bonding considerations, it would appear to implicate a differing influence of coadsorbed hydrogen and water on Pt(100).

The last example is for Pt(111). Similar θ_{CO}-dependent bridging/terminal CO site occupancies are observed for the Pt-

(55) Xu, Z.; Yates, J. T.; Kreuzer, J.; Wang, L. C. To be published.
(56) For example, see: Trasatti, S. *Electrochim. Acta* **1983**, *28*, 1083.
(57) (a) Tüshaus, M.; Schweizer, E.; Hollins, P.; Bradshaw, A. M. *J. Electron Spectrosc. Relat. Phenom.* **1987**, *44*, 305. (b) Schweizer, E.; Persson, B. N. J.; Tüshaus, M.; Hoge, D.; Bradshaw, A. M. *Surf. Sci.* **1989**, *213*, 49.
(58) Gurney, B. A.; Richter, L. J.; Villarrubia, J. S.; Ho, W. *J. Chem. Phys.* **1987**, *87*, 6710.
(59) Gardner, P.; Martin, R.; Tüshaus, M.; Bradshaw, A. M. *J. Electron Spectrosc. Relat. Phenom.* **1990**, *54/55*, 619.

(111)–aqueous interfaces at potentials corresponding to the predominant presence of water and hydrogen coadsorption.[16a] This finding by itself suggests that any specific effects of coadsorbed water and hydrogen, if present, are comparable. However, detailed measurements of θ_{CO}-dependent dipole–dipole coupling, as discerned from experiments with various $^{13}CO/^{12}CO$ mixtures, indicate that the CO adlayer structures at intermediate coverages for these two conditions are significantly different.[16a] Thus, the terminal ν_{CO} frequency upshifts due to dynamic dipole–dipole coupling, $\Delta\nu_D$, at intermediate dosed CO coverages are larger in the presence of water than hydrogen coadsorption, approaching the $\Delta\nu_D$ values (ca. 30 cm^{-1}) for saturated adlayers.[16a] These findings suggest that CO island formation for dosed adlayers, involving "patches" of CO having higher local coverages, is more prevalent in the presence of coadsorbed water than with hydrogen, resulting perhaps from the repulsive H_2O–CO coadsorbate interactions which have been noted for the corresponding Pt(111)–uhv system.[60] Further evidence regarding such specific roles of coadsorbed water or hydrogen, derived from metal–uhv systems, is noted below.

Water Coadsorption at Metal–UHV Interfaces: "Electrochemical Modeling". Several studies have been reported recently that examine the effects of water coadsorption on ν_{CO} spectra at metal–uhv interfaces.[60-62] Wagner et al. investigated the coadsorption of water and CO at subsaturated θ_{CO} values on Pt(111) and Rh(111) at 100 K.[60] The presence of water ($\lesssim$1 langmuir), either post- or predosed, yielded substantial alterations in the CO coordination geometry. For Pt(111), 2-fold bridging CO was induced to appear at low coverages, $\theta_{CO} \sim 0.2$, where the terminal form is otherwise exclusively present. The behavior on Rh(111) is noteworthy in that 1 langmuir of coadsorbed water yielded a near-complete shift of CO binding from the terminal to an apparently 3-fold bridging site, with $\nu^b_{CO} \approx 1620$–1700 cm^{-1}. This was attributed to "hydrophilic" CO/H_2O coadsorption, where CO and water form a mixed surface phase.

The latter finding is distinctly different from the behavior of the electrochemical Rh(111) interface at low θ_{CO} noted above, where terminal CO binding predominates in the presence of coadsorbed water. Nevertheless, the water-induced appearance of bridging as well as terminal CO at the Pt(111)–uhv interface at lower θ_{CO} mimics closely spectra observed for the corresponding electrochemical system. Related results have also been reported recently for the Rh(100)–uhv interface, where water coadsorption at subsaturated θ_{CO} values is seen to shift the site occupancy partly from terminal to 2-fold bridging so to resemble more closely infrared spectra for the Rh(100) electrochemical surface.[62] However, no changes in site occupancy were observed under these conditions for saturated ($\theta_{CO} \approx 0.75$) CO adlayers.

In light of the above discussion, interpretation of such coadsorbate-induced site occupancy shifts in terms of surface stereochemical factors or specific coadsorbate interactions should be tempered by a consideration of electrostatic field effects. That is, unlike electrochemical systems where ϕ^M is necessarily controlled externally, coadsorption of water as well as other species may well influence the adlayer structure at least partly via the consequent alterations in the surface potential. Thus, adsorption of water commonly yields large (ca. 0.5–1 eV) work function decreases on clean surfaces, reflecting a net orientation of the oxygen toward the metal along with adsorbate–surface charge transfer.[63] Although no work function measurements for coadsorbed water/CO systems have apparently been reported, one might anticipate that comparable ϕ^M decreases would also result from water dosing in this case, at least at low θ_{CO} values. On this basis, then, there is good reason to expect substantial *potential-induced* changes in both ν_{CO} frequency and site occupancy to result from water coadsorption in metal–uhv systems. Indeed, significant (ca. 20 cm^{-1}) decreases in ν^b_{CO} are induced on Pt(111) by water coadsorption,[60,61] although this may partly arise from diminutions in the extent of dipole–dipole coupling as the terminal site occupancy is lowered. The occurrence of surface-potential effects may therefore account, at least in part, for the increasing ν_{CO} spectral similarities observed between related electrochemical and metal–uhv interfaces in the presence of coadsorbed water, independent of additional "specific solvation" or coadsorbate stereochemical factors.

Such water coadsorption studies in uhv, examined with electrode systems in mind, are an example of "electrochemical modeling", whereby various components of electrode–solution interfaces can be constituted in uhv environments by gas-phase dosing. Such tactics, pioneered by Sass and co-workers,[64a] form a valuable means of examining incrementally the influence of different double-layer components on the interfacial properties. A limitation is that the surface temperature must be held below ca. 150 K in order to avoid water desorption, so that there is an inherently large temperature disparity between the "synthetic double layers" formed in uhv and the analogous electrochemical systems. Nonetheless, in addition to solvent dosing, the electrode charge and the ionic double-layer components can be synthesized by coadsorption of suitably ionized (or ionizable) species.[64,65]

So far, however, most vibrational spectroscopic studies concerned with "electrochemical modeling" have been limited to solvent coadsorption. An example of the likely important role played by the free-charge component of the double layer is the lack of additional bridging CO on Rh(100) induced by water dosing onto a *saturated* CO adlayer (vide supra).[62] At least under these conditions, the large ν_{CO} spectral differences remaining between the electrochemical and water-dosed uhv environments probably result primarily from the g^M_s(ion) component of the double-layer potential drop. In addition, as noted above, the presence of g^M_s(ion) can modify substantially the solvent dipolar potential. We reemphasize that adsorption (and coadsorption) in electrochemical systems, unlike metal–uhv interfaces, is usually undertaken at a controlled electrode potential. As a consequence, any alterations in surface potential resulting from adsorption of dipolar species, as discerned by work function changes in uhv systems, are *automatically canceled* in electrochemical interfaces by concomitant changes in the free-charge component of the surface potential, g^s(ion), so to maintain constancy of E^M (eq 1). Further discussion of these points, however, awaits the results of uhv experiments involving both appropriate ion and solvent dosing, along with work function measurements.

Hydrogen Coadsorption at Metal–UHV Interfaces. In addition to water, hydrogen coadsorption in uhv is of particular relevance to electrochemical systems given that high coverages of adsorbed atomic hydrogen are commonly formed at transition metal–aqueous interfaces at potentials approaching the onset of cathodic hydrogen evolution. The coadsorption of hydrogen and CO at metal–uhv interfaces has recently received substantial attention, particularly with regard to the distinction between microscopically "mixed" and "segregated" coadsorbate adlayers.[66] In the latter variant, microscopically separate domains are formed, consisting of the pure adlayer components. Crystallographically close-packed [such as (111)] surfaces tend to favor the formation of segregated CO and H domains, while the more open (100) and (110) faces (for face-centered cubic metals such as Pt and Rh) yield typically mixed CO/H adlayers.[66] Either segregated or mixed adlayers, however, can be produced for some systems, depending on the

(60) Wagner, F. T.; Moylan, T. E.; Schmieg, S. J. *Surf. Sci.* **1988**, *195*, 403.
(61) Tornquist, W. J.; Griffin, G. L. *J. Vac. Sci. Technol.* **1986**, *A4*, 1437.
(62) Leung, L.-W. H.; Goodman, D. W. *Langmuir* **1991**, *7*, 493.
(63) (a) For a review on water adsorption, see: Thiel, P. A.; Madey, T. E. *Surf. Sci. Rep.* **1987**, *7*, 211. Also see, for example: (b) Langenbach, E.; Spitzer, A.; Lüth, H. *Surf. Sci.* **1984**, *147*, 179. (c) Fusy, J.; Ducros, R. *Surf. Sci.* **1986**, *176*, 157.
(64) (a) Sass, J. K.; Bange, K. *ACS Symp. Ser.* **1988**, *No. 378*, 54 and earlier references quoted therein. (b) Wagner, F. T.; Moylan, T. E. *ACS Symp. Ser.* **1988**, *No. 378*, 65.
(65) (a) Kizhakevariam, N.; Döhl-Delze, R.; Stuve, E. M. *J. Phys. Chem.* **1990**, *94*, 5934. (b) Kizhakevariam, N.; Stuve, E. M.; Döhl-Delze, R. *J. Chem. Phys.* **1991**, *94*, 670.
(66) For reviews, see: (a) White, J. M.; Akhter, S. *CRC Crit. Rev. Solid State Mater. Sci.* **1988**, *14*, 131. (b) White, J. M. *J. Phys. Chem.* **1983**, *87*, 915.

formation conditions (e.g., ref 67).

While the use of vibrational spectroscopies for characterizing such systems has been rather limited, of interest in the present context are studies of CO/H coadsorption on Pt(111)[68] and on Rh(100)[67] using IRAS and EELS, respectively. The generation of substantial bridging CO upon the addition of hydrogen to low CO coverages on Pt(111) has been interpreted in terms of the formation of segregated CO domains having higher local coverages.[68] This interpretation, consistent with earlier information from thermal energy atom scattering,[69] is similar to that offered for CO/H_2O coadsorption on Pt(111).[60] It is also possible that surface potential effects, as considered above for H_2O coadsorption, play a role in the Pt(111)/CO,H uhv system in that hydrogen adsorption lowers significantly, by up to 0.35 V, the Pt(111) work function.[70] This markedly increased preference for bridge-bound CO on Pt(111) in the presence of hydrogen in uhv nonetheless suggests that the analogous behavior seen at low θ_{CO} in the electrochemical system is in part due to a stereochemical influence of the coadsorbate.

The structures and site occupancies for CO coadsorbed with hydrogen on Rh(100) in uhv as deduced by EELS and LEED are particularly sensitive to the experimental conditions,[67] in that either mixed or segregated adlayers, and dominant terminal as well as 2-fold bridging CO coordination, can be obtained. This behavioral complexity probably reflects the very similar binding energetics of CO in the terminal and 2-fold bridging sites on this surface in uhv.[53,54] For the corresponding Rh(100)/CO electrochemical system, however, 2-fold bridging CO coordination dominates for subsaturated CO adlayers in the presence of both coadsorbed hydrogen and water. On the basis of the above arguments, the latter findings are consistent with the markedly (ca. 1–2 V) lower potentials that characterize the electrochemical Rh(100) interface. Work function measurements for the Rh(100)/CO,H uhv system show that while ϕ^M is up to ca. 0.6 V lower in the presence of coadsorbed H than with CO adsorbed alone, the surface potential is nevertheless increased above the clean surface value (5.0 V) upon H/CO coadsorption.[71]

The observed marked sensitivity of the CO site occupancy at the Pt(100) electrochemical interface to the presence of hydrogen versus water coadsorption as well as to variations in θ_{CO} and E^M, noted above,[16b] bears a similarity to the behavior of the Rh(100) surface in uhv. The resemblance probably reflects the near equality of the binding energies for 2-fold bridging and terminal binding on Pt(100) at the potentials ($\phi^M \sim 3.8$–4.8 V, Figure 3) that are encountered in the aqueous electrochemical system, mirroring the similar situation on Rh(100) at the higher surface potentials that characterize the uhv surface environment (vide supra).[53]

Metal Coadsorption. Besides the inevitable occurrence of water and hydrogen coadsorption in aqueous electrochemical systems, the effects of metal adatoms on molecular adsorption are of particular interest. As for corresponding "bimetallic" interfaces in uhv,[72] their significance derives in part from the dramatic modification in surface electronic, and catalytic, properties that can be afforded in this manner. We describe here briefly the effect of bismuth coadsorption in CO binding to platinum low-index electrodes in relation to corresponding uhv results.[19]

The adsorption of bismuth on platinum is an especially suitable system since irreversible binding can be affected by prior immersion into dilute Bi^{3+} solutions, and the resulting adlayer coverages can be quantified from the charge required for their reversible electrooxidation.[19,73] Such predosed bismuth adlayers on Pt(111) in aqueous 0.1 M $HClO_4$ yield CO adsorption preferentially into terminal rather than bridging sites; at the saturation bismuth coverage, $\theta_{Bi} = 0.21$, CO binding is exclusively terminal throughout the accessible θ_{CO} range, $\theta_{CO} \lesssim 0.37$.[19] These results indicate the presence of a microscopically intermixed coadsorbed layer, with bismuth bound to bridging sites that would otherwise be occupied by CO. Comparable behavior was also observed on Pt(100) in aqueous 0.1 M $HClO_4$.[19]

Adsorption of CO onto Pt(111) with predosed bismuth in uhv yields somewhat different results.[74] While an intermixed adlayer is apparently also formed, increasing θ_{Bi} yields correspondingly smaller θ_{CO} values which nonetheless exhibit little change in the terminal/bridging site occupancies as discerned from EELS.[74] However, there are substantial (100–200 cm^{-1}) downshifts in ν^t_{CO} and especially in ν^b_{CO} as θ_{Bi} is increased, contrasting the small frequency alterations observed for the electrochemical system under these conditions.[19] The former frequency downshifts, however, are unsurprising on the basis of the large (up to 2 eV) work function decreases known to accompany bismuth adsorption on Pt(111).[74] Such marked changes in surface potential can also rationalize the maintenance of bridging CO coordination in the presence of coadsorbed bismuth on Pt(111) in uhv. The marked preference for terminal CO coordination under these conditions in the electrochemical system can be attributed to the constancy of the electrode potential, enabling the stereochemical factors that favor this coordination in the mixed adlayer to be disentangled from the effects of electrostatic fields and surface bonding that inevitably vary as the surface potential is altered, as in the uhv case. Admittedly, however, the behavioral differences between the electrochemical and uhv systems may well reflect in part intrinsic differences in the bismuth adlayer structures in these two environments.[19]

Further Developments and Future Prospects

Although the range of chemical systems examined so far is rather narrow, it is apparent that the detailed in situ infrared characterization of monocrystalline metal–solution interfaces can, especially when combined with vibrational data for related metal–uhv surfaces, yield substantial new insight into the microscopic structural factors that control both types of interfacial environment. Besides the recent emergence of reliable means of preparing ordered monocrystalline surfaces for in situ electrochemistry, a major impetus is provided currently by the growing recognition by surface scientists of the power of infrared spectroscopy for detailed adsorbate structural characterization.[75]

A reoccurring theme in the above discussion, in particular, involves the importance of the surface potential in controlling the interfacial structure via the electrostatic field and/or electronic effects on the surface bonding. While these notions are familiar (if not always understandable) to electrochemists given the pivotal conceptual status of the electrode potential and charge in surface electrochemistry, researchers in uhv surface science tend to be less acquainted with the role and importance of these factors. Moreover, reliable evaluation of the surface potential (via the work function) in metal–uhv systems is not yet commonplace, even when an avowed aim is to relate the observed behavior to that of electrochemical systems. Consequently, then, the quantitative comparison of potential-dependent ν_{CO} frequencies and CO binding geometries pursued above between related electrochemical and metal–uhv surfaces is limited largely to examples of the latter for which coadsorption is absent. It will clearly be of interest to examine infrared spectra for CO at metal–uhv interfaces dosed with both solvent and ionizable species so to yield a sequence of ϕ^M values that span those encountered in the corresponding electrochemical systems. While the ambient temperatures en-

(67) (a) Richter, L. J.; Gurney, B. A.; Ho, W. *J. Chem. Phys.* **1987**, *86*, 477. (b) Richter, L. J.; Germer, T. A.; Ho, W. *Surf. Sci.* **1988**, *195*, L182.
(68) Hoge, D.; Tüshaus, M.; Bradshaw, A. M. *Surf. Sci.* **1988**, *207*, L935.
(69) (a) Bernasek, S. L.; Lenz, K.; Poelsema, B.; Comsa, G. *Surf. Sci.* **1987**, *183*, L319. (b) Lenz, K.; Poelsema, B.; Bernasek, S. L.; Comsa, G. *Surf. Sci.* **1987**, *189/190*, 431.
(70) Christmann, K.; Ertl, G. *Surf. Sci.* **1976**, *60*, 365.
(71) (a) Kim, Y.; Peebles, H. C.; White, J. M. *Surf. Sci.* **1982**, *114*, 363. (b) Peebles, D. E.; Peebles, H. C.; White, J. M. *Surf. Sci.* **1984**, *136*, 463.
(72) For recent reviews, see: (a) Campbell, C. T. *Annu. Rev. Phys. Chem.* **1990**, *41*, 775. (b) Goodman, D. W. *ACS Symp. Ser.* **1989**, *No. 411*, 191.
(73) Clavilier, J.; Feliu, J. M.; Aldaz, A. *J. Electroanal. Chem.* **1988**, *243*, 419.
(74) Paffett, M. T.; Campbell, C. T.; Windham, R. G.; Koel, B. E. *Surf. Sci.* **1989**, *207*, 274.
(75) For example, see: *Vibrations at Surfaces 1990*; Chabel, Y. T., Hoffmann, F. M., Williams, G. P., Eds.; Elsevier: Amsterdam, 1990; published in: *J. Electron Spectrosc. Relat. Phenom.* **1990**, *54/55*.

countered for the latter systems cannot be mimicked readily by the former, such experiments offer the intriguing prospect of discerning in stepwise fashion the relationships between the ν_{CO} frequencies and site occupancies with ϕ^M as the latter is varied by altering *separately* the free-charge and dipolar components of the surface potential.

One issue to be addressed is the extent to which the CO surface bonding is dependent upon specific factors, such as the nature of the dipolar solvent and/or the solvated ions, rather than the inherently nonspecific surface potential drop. At least for saturated ($\theta_{CO} \approx 0.7$) CO adlayers on Pt(111), closely similar $\nu^L_{CO}-\phi^M_s$ and $\nu^b_{CO}-\phi^M_s$ plots are obtained in a range of solvents, including water and aprotic media such as acetonitrile, in the presence of a given supporting electrolyte.[37] These findings suggest that the solvent exerts little influence on the adlayer properties once a given surface potential ϕ^M has been established. Quite different results, however, might be anticipated at lower CO coverages where solvent coadsorption can occur.

Alongside such experimental developments, there is a need for more sophisticated theoretical–computational approaches that can describe, at least semiquantitatively, the combined effects of electrostatic fields and surface bonding on the adsorbate stability and vibrational properties for specific binding sites. While most attention has justifiably been devoted so far to carbon monoxide as an adsorbate probe molecule, other systems could be examined both experimentally and theoretically, with the aim of expanding the range of surface chemistry amenable to in situ vibrational spectroscopy in related electrochemical and uhv environments.

One rich class of interfacial systems, which has so far been virtually unexplored in the present context, involves bimetallic surfaces formed by submonolayer metal deposition onto an ordered substrate. As noted above, such bimetallic systems offer a valuable means of altering systematically the electronic and stereochemical bonding properties of monocrystalline metal surfaces.[72] It will be of interest to examine adsorbate vibrational properties on related bimetallic interfaces (such as bismuth adlayers noted above) formed by either electrochemical or vapor-phase deposition[76] and examined interchangably in both surface environments by using transfer techniques.

Such bimetallic systems form one important class of interfaces of interest in electrocatalysis. Although lying outside the scope of the present article, time-resolved FTIR techniques can be utilized for the examination of well-defined surfaces while electrocatalytic reactions are proceeding, providing significant mechanistic insight.[22,77] These studies are analogous to the emerging use of FT-IRAS for following catalytic processes at metal–gas interfaces at relatively high pressures.[78] It is worth noting that the connection between fundamental adsorption and catalytic studies at electrochemical interfaces is intrinsically closer than for metal–uhv surfaces since the "pressure gap" between uhv and catalytically relevant (i.e., higher pressure) conditions for the latter systems does not exist for the former.

While infrared spectroscopy is so far an unusual example of a molecular-level technique applicable to both in situ electrochemical and uhv surface environments, other microscopic approaches may be exploited to provide common structural and bonding information. In particular, scanning tunneling microscopy (STM) can be utilized to provide real-space structures with atomic resolution in favorable cases at both types of metal surfaces. Recent evidence that saturated CO adlayers can be imaged with STM on monocrystalline metal–aqueous interfaces[79] provides the intriguing prospect of employing IRAS and STM in tandem as complementary structural probes of electrochemical adsorbate–surface bonding. Indeed, detailed atomic-level analyses of CO adlayer structure have already been pursued along these lines on rhodium low-index electrodes.[80]

Overall, then, there is good reason to expect that the long-standing, if narrowing, gulf in understanding (and treatments) of structure and bonding phenomena at metal–solution and metal–uhv interfaces will be bridged further by the concerted application of such microscopic techniques to systems and issues of common interest to both areas. Consequently, then, we anticipate that these emerging links between electrochemical and metal–uhv interfaces will contribute increasingly and substantively to an enhanced commonality of understanding in surface science.

Acknowledgment. Lam Leung contributed importantly to the initial development of infrared spectroscopy at monocrystalline electrodes in our laboratory. We are also grateful to Andrzej Wieckowski and Antoinette Hamelin for expert advice and encouragement regarding single-crystal electrochemistry. We thank David Lambert, Eric Stuve, and John Yates for communicating results prior to publication and for helpful discussions and comments on this manuscript. Valuable comments were also supplied by Sergio Trasatti. S.C.C. acknowledges the W. R. Grace Foundation and the Analytical Division of the American Chemical Society for graduate fellowships. This work is supported by the National Science Foundation.

Registry No. CO, 630-08-0; Pt, 7440-06-4; Rh, 7440-16-6; $HClO_4$, 7601-90-3; water, 7732-18-5; hydrogen, 1333-74-0.

(76) For example, see: Stuve, E. M.; Rogers, Jr., J. W.; Ingersoll, D.; Goodman, D. W.; Thomas, M. L.; Paffett, M. T. *Chem. Phys. Lett.* **1988**, *149*, 557.

(77) Chang, S.-C.; Hamelin, A.; Weaver, M. J. *J. Chim. Phys.*, in press.

(78) For example, see: Hoffmann, F. M.; Weisel, M. W.; Peden, C. H. F. *J. Electron Spectrosc. Relat. Phenom.* **1990**, *54/55*, 779.

(79) Yau, S.-L. Ph.D. Thesis, Purdue University, Dec 1990.

(80) (a) Yau, S.-L.; Gao, X.; Chang, S.-C.; Schardt, B. C.; Weaver, M. J. *J. Am. Chem. Soc.*, in press. (b) Gao, X.; Vitus, C.; Yau, S.-L.; Weaver, M. J. Manuscript in preparation.